Accepted Manuscript

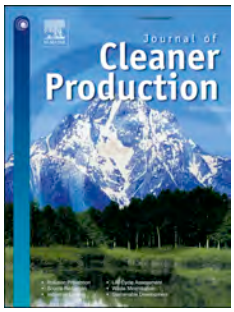

Upcycling carbon dioxide to improve mechanical strength of Portland cement

Ling Qin, Xiaojian Gao, Qiyan Li

PII: S0959-6526(18)31770-0

DOI: 10.1016/j.jclepro.2018.06.120

Reference: JCLP 13266

To appear in: *Journal of Cleaner Production*

Received Date: 24 April 2018

Revised Date: 7 June 2018

Accepted Date: 11 June 2018

Please cite this article as: Qin L, Gao X, Li Q, Upcycling carbon dioxide to improve mechanical strength of Portland cement, *Journal of Cleaner Production* (2018), doi: 10.1016/j.jclepro.2018.06.120.

Word count: 6876

Upcycling carbon dioxide to improve mechanical strength of Portland cement

Ling Qin[a], Xiaojian Gao[a, b]*, Qiyan Li[a]

[a] School of Civil Engineering, Harbin Institute of Technology, Harbin 150090, China
[b] Key Lab of Structures Dynamic Behavior and Control of the Ministry of Education, Harbin Institute of Technology, Harbin 150090, China

*Correspondence: E-mail: gaoxj@hit.edu.cn; Tel.: +86-451-86281118; Fax: +86-451-86281118.

Abstract: To reduce environmental pollution induced by the production of Portland cement and sequestrate greenhouse gas, a novel approach was developed to manufacture nano-calcium carbonate (nano-$CaCO_3$) suspension by upcycling carbon dioxide. The influence of this nano-$CaCO_3$ suspension on basic performances of Portland cement paste was experimentally evaluated and related mechanisms were demonstrated by isothermal heat conduction calorimeter (TAM Air), X-ray diffraction (XRD), Fourier transform infrared spectroscopy (FTIR), thermogravimetry-differential thermal analysis (TG-DTA), mercury intrusion porosimeter (MIP), scanning electron microscope (SEM) and transmission electron microscope (TEM) measurements. Experimental results showed that the manufactured $CaCO_3$ presented spherical and cubic shapes with size of 20 to 50 nm. This CO_2 upcycling method can improve compressive strength of cement paste by 5.8~9.9% at ages of 3 to 56 days and significantly reduce the initial and final setting times. The introduction of CO_2 in form of nano-$CaCO_3$ accelerated the early age hydration of Portland cement and refined the pore structure. Around 0.4~2.4 kg of CO_2 can be recycled by every ton of Portland cement while the usage efficiency of cement was evidently improved. Therefore, both capture and solidification of carbon dioxide and carbon footprint reduction of cement industry can be simultaneously achieved by this technology.

Keywords: CO_2 recycling; Nano-$CaCO_3$; Portland cement; Compressive strength; Hydration behavior.

1. Introduction

It is well known that Portland cements (PC) is one of the most widely used materials for construction of buildings and other infrastructures (Biernacki et al., 2017； Schneider et al., 2011; Shi et al., 2011). The reported worldwide production of Portland cements reached as high as 4.6 billion tons in 2016, of which more than 60% was contributed by China (CEMBUREAU, 2016). The PC production is a typical CO_2 release and energy consumption process, being responsible for nearly 9% of anthropogenic CO_2 emission and accounts for approximately 3% of the global energy use (Shi et al., 2011). Generally speaking, around one ton of CO_2 is discharged by the production of every ton PC (Hemalatha and Ramaswamy, 2017) and such CO_2 emission is attributable to two aspects. On the one hand, CO_2 is a by-product from the calcination of limestone to create reactive calcium silicates (Shi et al., 2011; Vance et al., 2015); on the other hand, the combustion of fossil fuel required for clinkering raw materials (clay and limestone) at 1450 ℃ also releases a great deal of CO_2 (Vance et al., 2015). Therefore, the carbon impact of Portland cement industry has attracted increasing attentions and many efforts have been carried out to address a lower-carbon or greener production of cements (Bourtsalas et al., 2018; Benhelal et al., 2018; Carvalho et al., 2017).

The cement concrete industry worked with the International Energy Agency to outline the ambitious effort to decrease industrial emissions to 50% below levels of 2006 till 2050 (Monkman and Macdonald, 2017). It is in accordance with the “blue map scenario” (International Energy Agency, 2008). There are four suggested approaches for achieving this target (Monkman and Macdonald, 2017): to improve the energy efficiency of cement kilns, to increase the usage of low-carbon supplementary cementitious materials (SCMs) to replace clinker, to utilize alternative raw materials and/or fuels for manufacture of Portland clinker and to capture or sequestrate CO_2. The first three methods have been

commonly applied in many countries, but are sometimes restricted by the local availability of recyclable resources (Scrivener, 2014) and regional technology level (Madlool et al., 2013). Therefore, the carbon capture and sequestration (CCS) technology is regarded as the greatest potential for the carbon reduction project. Nevertheless, it is still an undefined measure developed outside the cement industry (Scrivener et al., 2016). Several researches demonstrated that the lower carbon cement and concrete products can be prepared using concepts of CO_2 utilization (Ashraf, 2016; Jang et al., 2016; Zhang et al., 2017) and many efforts focused on maximizing the sequestered amount of CO_2 within useful building products (Monkman and Macdonald, 2017). The carbonation curing was reported as an effective method to improve strength (Monkman and Shao, 2010; Ahmad et al., 2017) and durability of cement-based materials (Rostami et al., 2011). Nevertheless, there is still a major obstacle for this technique that is carbonation speed. The diffusion of CO_2 into the concrete matrix is very slow which causes the low carbonation speed. Furthermore, as the main carbonation product, $CaCO_3$ can fill the pores in concrete matrix and results in the more difficult diffusion of CO_2 (Kashef-Haghighi and Ghoshal, 2013). In addition, the later age compressive strength of concrete is possibly decreased due to the water loss during carbonation curing period (El-Hassan and Shao, 2015). Therefore, further studies should be carried out in the field of carbonation curing.

In latest years, considerable progresses have been achieved in the field of ‘nano-concrete’ (Nazari and Riahi, 2011; Sanchez and Sobolev, 2010), being related to incorporating different types of active or inactive fillers with nano-level sizes. As an easily available mineral, nano-$CaCO_3$ attracts more and more interests in the scientific community. It has been found that a low amount of nano-$CaCO_3$ behaves an accelerating effect on the hydration and strength gain of cements and concretes (Sato and Beaudoin, 2011; Sato and Diallo, 2010). However, the actual obstacle to incorporating nano-$CaCO_3$

into cement-based materials is the difficulty of dispersion due to the high surface energy (Kawashima et al., 2013). In this case, the potential of nanofillers could not be fully activated or even a negative effect on mechanical strength of cement concrete occurs (Cai et al., 2017).

In order o address the limitations in the existing methods summarized above, this paper developed an innovative approach to upcycle CO_2 for manufacturing a homogeneous nano-$CaCO_3$ suspension as a mineral additive for Portland cement. The procedure provides a simple and convenient method for capturing and sequestrating CO_2, involving the injection of CO_2 into a $Ca(OH)_2$ solution with a low-cost equipment. On the other hand, the incorporation of this nano-$CaCO_3$ suspension behaved a significant increasing effect on mechanical strength of Portland cement paste, resulting in the increased usage efficiency of Portland cement. Both these two aspects are favorable for the cleaner production of Portland cement. The mechanism of nano-$CaCO_3$ suspension in Portland cement system was demonstrated by isothermal heat conduction calorimeter (TAM Air), X-ray diffraction (XRD), Fourier transform infrared spectroscopy (FTIR), thermogravimetry-differential thermal analysis (TG-DTA), mercury intrusion porosimeter (MIP), scanning electron microscope (SEM) and transmission electron microscope (TEM) measurements.

2. Materials and methods

2.1 Raw materials

The PC used in this study is produced by Dalian Cement Group with strength grade of 42.5 in accordance with Chinese standard GB 175-2007. The particle size distribution of this cement is presented in Fig. 1 with D50 value of 18.73 μm. The chemical composition was analyzed by X-ray fluorescence (XRF) test as shown in Table 1. Hydrated lime with an analytical purity was used to prepare $Ca(OH)_2$ solution and a commercially available CO_2 gas with 100% concentration was

adopted.

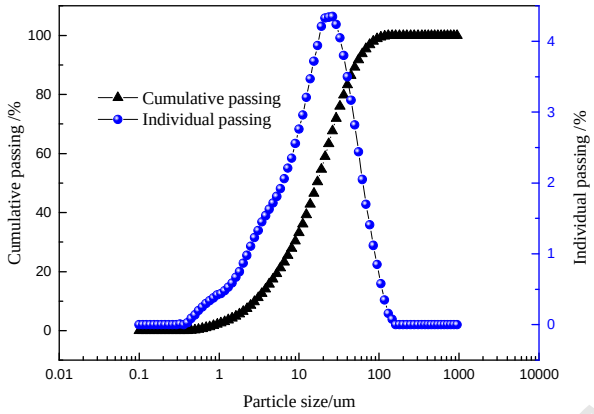

Fig. 1. Particle size distribution of the used PC.

Table 1 Chemical composition of PC (wt %).

Component	CaO	SiO_2	SO_3	Fe_2O_3	Al_2O_3	MgO	K_2O	Loss of ignition
Content	64.60	17.38	4.52	3.99	3.27	2.62	0.65	2.97

2.2 Mixing proportion and specimen preparation

Cement pastes with water-binder ratio of 0.4 were prepared as described by the flowchart in Fig. 2. Firstly, $Ca(OH)_2$ was dissolved into deionized water to form $Ca(OH)_2$ solutions with concentrations of 0.17% (B1), 0.34% (B2) and 1.02% (B3) by mass. Secondly, CO_2 was added into $Ca(OH)_2$ solutions by a mobile gas injection system at a specified flow rate of 20 L/min. This injection operation lasted for 150 seconds for every liter of solution (or 30 seconds for every 500 g PC). An additional 30 seconds of high speed mixing followed the injection to obtain a homogeneous suspension. After this operation, the nano-$CaCO_3$ suspension was prepared by the reaction of CO_2 and $Ca(OH)_2$ in solution. Thirdly, PC and $CaCO_3$ suspension were added in a pot with the mass ratio of 1:0.4 and then blended for 5 minutes using a planetary cement paste mixer. Finally, three flowable fresh cement pastes were obtained by incorporating nano-$CaCO_3$ and the control sample was also prepared by adding deionized water. As shown in Table 2, the equivalent dosage of $Ca(OH)_2$ are 0%, 0.068%, 0.136% and 0.408% by PC

weight respectively. As described in a previous study (Mo t al., 2016), specimens with dimensions of 20 mm × 20 mm × 20 mm were prepared for mechanical strength measurement. The casted specimens were covered with plastic sheets after consolidation and cured at 20±3 ℃ for 24 hours before demolding. The demolded specimens were then exposed to the standard curing room (22 ± 3℃, RH 90%) till strength measurement.

Table 2 Equivalent dosage of $Ca(OH)_2$ for introducing nano-$CaCO_3$.

No.	Control	B1	B2	B3
$Ca(OH)_2$ (wt%)	0	0.068	0.136	0.408

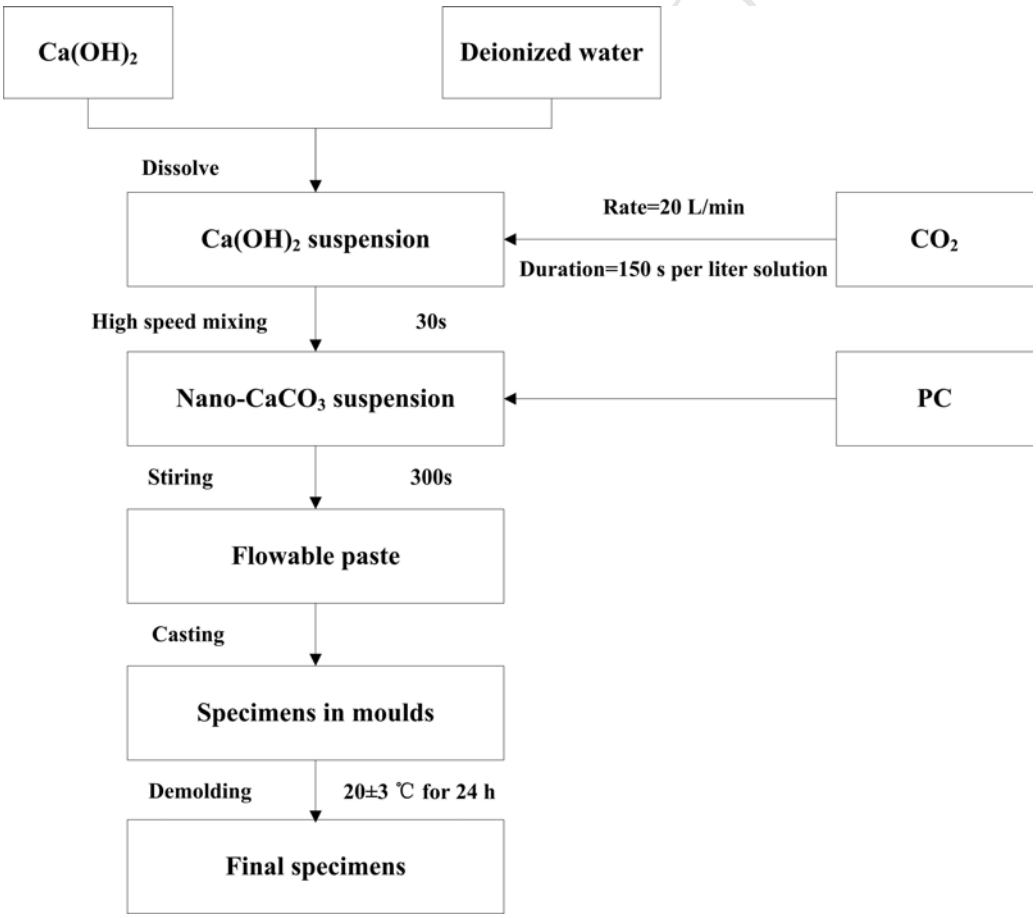

Fig. 2. Manufacture flowchart of PC specimens.

2.3 Test methods

The fluidity of cement paste was measured using a truncated cone with upper diameter of 36 mm,

base diameter of 60 mm and height of 60 mm in accordance with Chinese standard GB/T8077-2000. Setting time of cement pastes was determined by a Vicat apparatus in accordance with Chinese standard GB/T1346-2011. Compressive strength for every mixture was measured after 3, 7, 28 days and 56 days of curing, with a loading rate of 1.0 kN/s according to GB/T17671-1999. Six cubic specimens were tested for each group and the average value was recorded as the compressive strength.

To evaluate the influence of nano-$CaCO_3$ on hydration process of Portland cement, the hydration heat was determined on every mixture at 20 □ using an isothermal calorimetry (TAM Air) with a sensitivity of 0.4 μJ and a baseline stability of ±0.08 μW/h (Wadsö, 2005). The pH value of nano-$CaCO_3$ suspension was tested by a PHS-2C pH meter. To characterize the phase composition and microstructure of the prepared nano-$CaCO_3$ suspensions or cement paste, the following tests were carried out. XRD patterns were performed by an X'Pert PRO diffractometer with Cu-Kα radiation (λ = 0.15419 nm) over a 2θ range from 5° to 70°. The FTIR patterns were collected by a Fourier transform infrared spectrometer (FTIR-650) under the following conditions: 4252-250 cm^{-1} range, 2 cm^{-1} resolution. For FTIR measurement, KBr discs were prepared by pressing pellets containing 1 mg of tested sample and 100 mg of KBr. TG-DTA measurement was carried out by a thermal analyzer (NETZSCH, TG 449F3 Jupiter) with a resolution of 0.01 mg. Around 20 mg of dried powder sample were tested when the temperature increased from 20 to 1000 ℃ with a speed of 10 ℃/min. Pore size distribution of hardened cement pastes were tested using a IV 9510 mercury Intrusion porosimetry (MIP) with a pressure range from 0 to 60000 psi (414 MPa). The microstructure observation was performed on selected cement paste samples using a JEOL SX-4 scanning electron microscope (SEM) with an energy dispersive spectrometer (EDS) which was operated at an accelerating voltage of 30kV. The morphologies of the manufactured nano-$CaCO_3$ samples were investigated using a JEOL

JEM-2011 transmission electron microscope (TEM) with an acceleration voltage up to 120 kV, a magnification power up to 600 k and a resolving power down to 0.2 nm. Nano-$CaCO_3$ powders were collected by suction filtration using a Hirsch funnel and then immersed in pure ethanol and dispersed using an ultrasonic bath before TEM observation.

3. Results and discussion

3.1 Characterization of the manufactured nano-$CaCO_3$

Fig. 3 presents visual appearances of the manufactured nano-$CaCO_3$ suspensions. It looks like a white milky suspension and the turbidity was strengthened with the higher concentration of $Ca(OH)_2$. The pH values of these suspensions reached around 6.5 as shown in Table 3, conforming to the requirements for mixing water of concrete (higher than 4.0) specified by Chinese standard JGJ 63-2006.

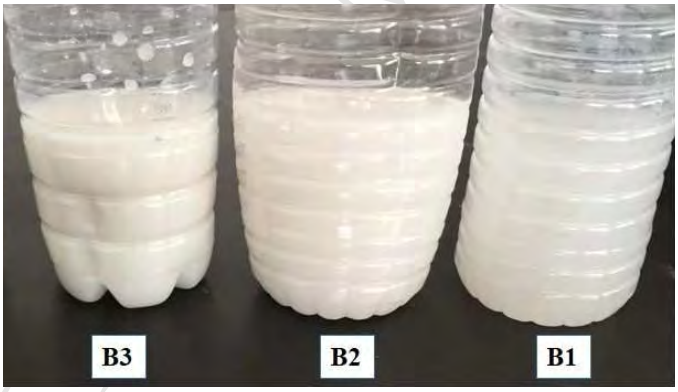

Fig. 3. Appearance of manufactured nano-$CaCO_3$ suspensions.

Table 3 pH values of manufactured nano-$CaCO_3$ suspension.

Group	B1	B2	B3
pH	6.57	6.46	6.45

Fig. 4 presents the XRD patterns of these manufactured nano-$CaCO_3$ suspension samples. It is evidently found that the mineral composition for every sample is $CaCO_3$, being induced by the chemical reaction of $Ca(OH)_2$ and CO_2 (Xi et al., 2015). And no evidence can be detected for the

existence of $Ca(OH)_2$ for every sample. The FTIR spectrum for every sample is presented in Fig. 5, in which the absorption bands corresponding to C-O and O-H can be easily identified. The peak at 3420 cm^{-1} is associated with the O-H stretching band due to the existence of water (H_2O) (Qin et al., 2018a, 2018b). Peaks at 713, 875 and 1430 cm^{-1} are assigned to the C-O bending and stretching bands and are attributable to the existence CO_3^{2-} (Shao et al., 2014). This can be confirmed by the formation of $CaCO_3$ as presented in XRD patterns.

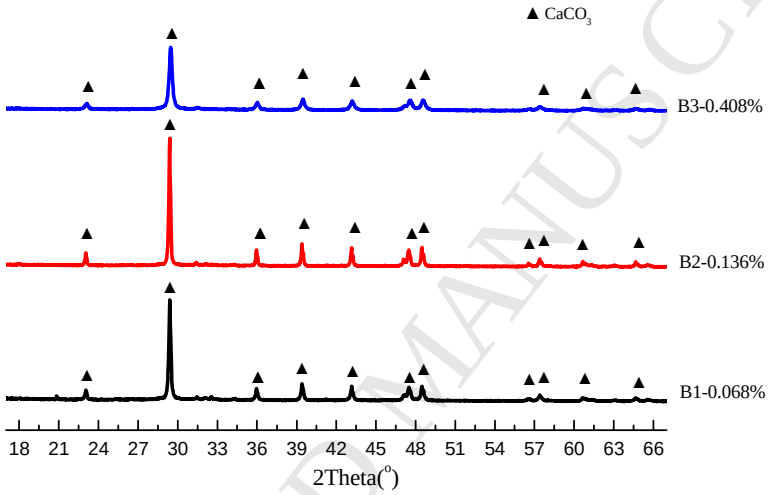

Fig. 4. XRD patterns of manufactured nano-$CaCO_3$ suspensions.

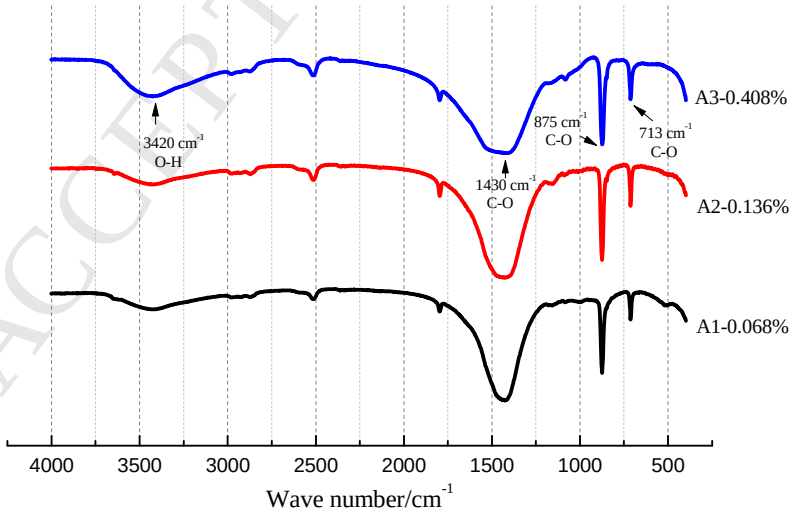

Fig. 5. FTIR spectra of manufactured nano-$CaCO_3$ suspensions.

From DTA-TG curves as indicated in Fig. 6, it can be found that every sample exhibited an

obvious endothermal peak at temperature around 800 ℃, corresponding to the decomposition of $CaCO_3$ (Mo et al., 2016; Rostami et al., 2012). At the same time, an obvious weight loss was induced by the decarbonation of $CaCO_3$ (Shao et al., 2014). It is also supported that no visible $Ca(OH)_2$ remained in every sample. Combined with the XRD results, it can be concluded that the substance $Ca(OH)_2$ in every solution was totally converted into $CaCO_3$ crystals after the CO_2 injection treatment. According to the mix proportion of cement paste, CO_2 was captured by 0.0404%, 0.0809% and 0.2426% of the PC weight for sample B1, B2 and B3 respectively.

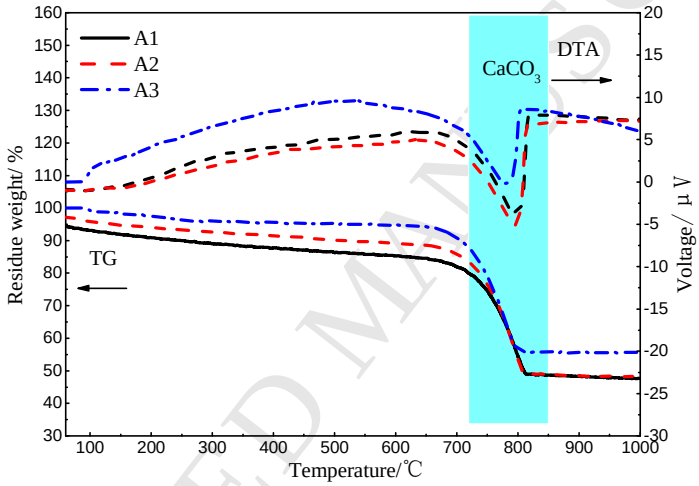

Fig. 6. DTA-TG curves of B1~B3 specimens.

TEM morphology observations for $Ca(OH)_2$ and manufactured nano-$CaCO_3$ are presented in Fig. 7. There were individual tetrahedral crystals with particle size of 138~200 nm and some larger agglomerated cube-like particles with size of 200-500 nm in the untreated $Ca(OH)_2$ solution sample. These findings are in accordance with other studies (Asikin-Mijan et al., 2015; Du et al., 2016). For sample B1, nano-$CaCO_3$ particles with a spherical morphology can be found and these particles had similar sizes of 20~50 nm. With the increasing concentration of $Ca(OH)_2$, the manufactured nano-$CaCO_3$ exhibited variable morphologies. For sample B2 and B3, there are many cubic particles with an average size of 35 nm and size range of 20 to 50 nm, indicating that the manufactured

186 nano-$CaCO_3$ behaved in the form of typical calcite crystals (Xi et al., 2015). The nano-$CaCO_3$ filler
187 with this type of cubic morphology was reported by other researchers (Sato and Beaudoin, 2011). It is
188 indicated that this CO_2 upcycling process provides a substitutable manufacture method of nano-$CaCO_3$
189 filler being applicable for cements. Nano-$CaCO_3$ particles behaved a higher tendency of agglomeration
190 for the higher concentration sample. This variable morphology and particle size is related to the
191 precipitation process (El-Sheikh et al., 2013), being attributed to many factors such as the initial
192 concentration of $Ca(OH)_2$, stirring effect due to the injection of CO_2 and sampling preparation
193 (El-Sheikh et al., 2013; Reddy and Nancollas, 1976). Therefore, further studies should be carried out in
194 the manufacture process to obtain a highly dispersed nano-$CaCO_3$ suspension.

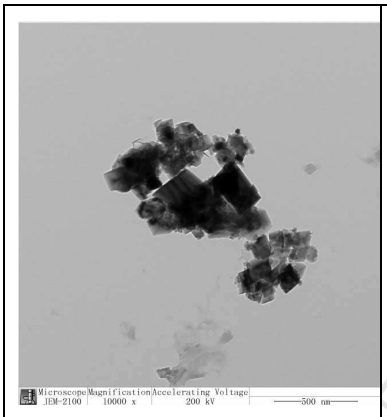

(a) $Ca(OH)_2$ (×10000)

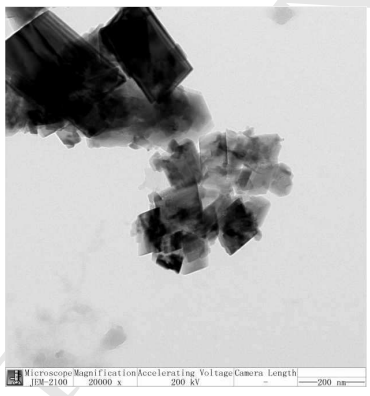

(b) $Ca(OH)_2$ (×20000)

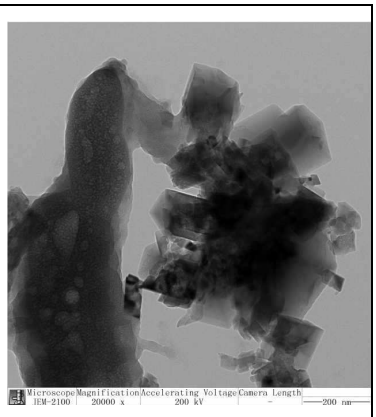

(c) $Ca(OH)_2$ (×20000)

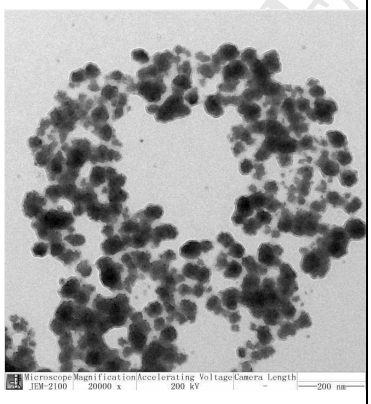

(d) B1 (×20000)

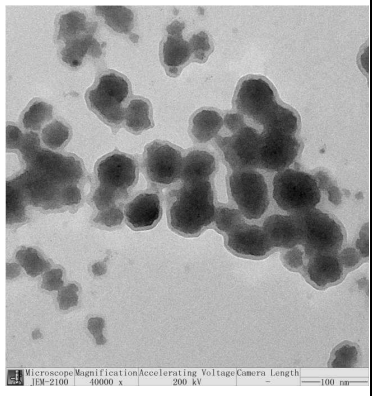

(e) B1 (×40000)

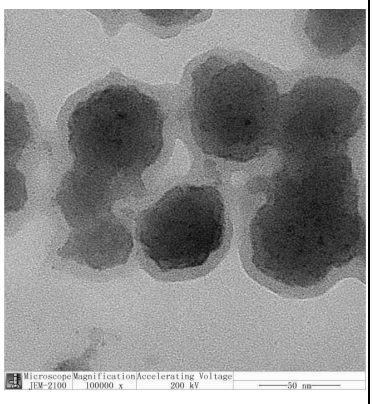

(f) B1 (×100000)

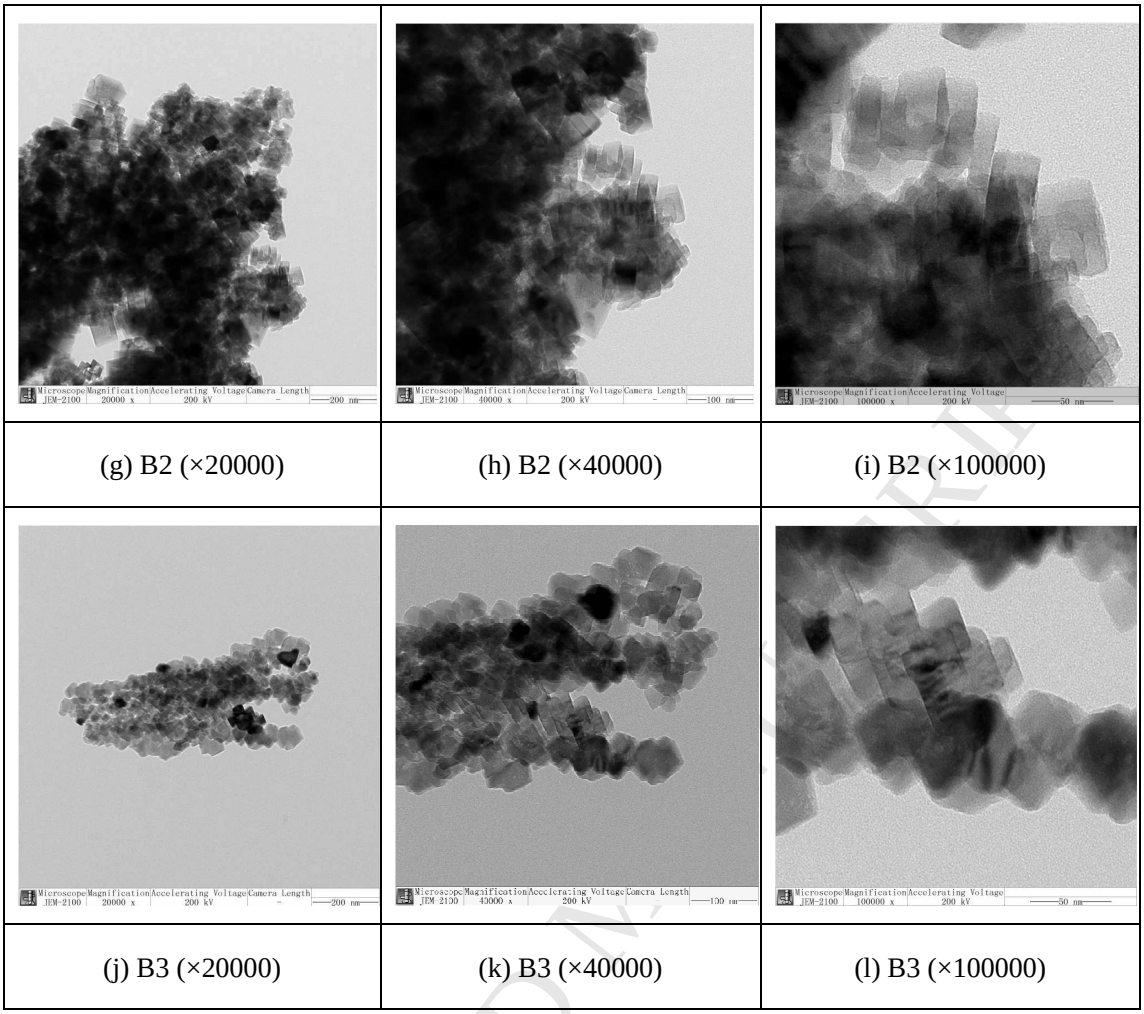

(g) B2 (×20000) (h) B2 (×40000) (i) B2 (×100000)

(j) B3 (×20000) (k) B3 (×40000) (l) B3 (×100000)

Fig. 7. TEM morphology observation of $Ca(OH)_2$ and manufactured nano-$CaCO_3$.

3.2 Fresh properties of cement paste

The fluidity and setting time of fresh cement pastes are shown in Fig. 8 and Fig. 9 respectively. As observed from Fig. 8, the fluidity of fresh cement paste was decreased by 3.95%~15.79% with the incorporation of nano-$CaCO_3$ suspensions and the higher dosage of nano-$CaCO_3$ led to the lower flowability. It was also reported that the addition of nano-Al_2O_3 reduced the mortar fluidity by 45% when the mixing amount was only 0.25 wt% (Liu et al., 2015). This is attributed to a layer of free water adsorbed by these nano-particles with large specific surface area. Therefore, more chemical admixture is needed or an additional amount of mixing water is required to fill the remaining voids among granular particles (Quercia et al., 2012). Several researchers found that there is a direct relationship

between water requirement and specific surface area of micro powders and a water layer with constant thickness of 25 nm formed for several tested micro powders (Brouwers, 2008; Brouwers and Radix, 2005).

As for the setting time, it can be found that nano-$CaCO_3$ suspensions had an evident shortening effect on the setting times of cement pastes. The initial and final setting time were decreased by 8.89%~30.22% and 7.89%~19.08% respectively. It is well known that the set of Portland cement is attributed to the formation of calcium silicate hydrate (C-S-H) from the hydration reaction of tricalcium silicate (Alite, C_3S) (Madani et al., 2012). The initial set coincides with the end of induction period of cement hydration (Double and Hellawell, 1978). Therefore, the decreased initial setting time of cement pastes, being observed in the presence of nano-particles (Kawashima et al., 2013; Senff et al., 2009), reflected the reduction of induction period. The final set of cement occurs around the middle point of the acceleration period of cement hydration (Double and Hellawell, 1978). Nano-$CaCO_3$ created additional surfaces for precipitation of hydrate products and accelerated the early age hydration of cement. The influence of these nano-$CaCO_3$ suspensions on the cement hydration will be fully described in Part 3.4.

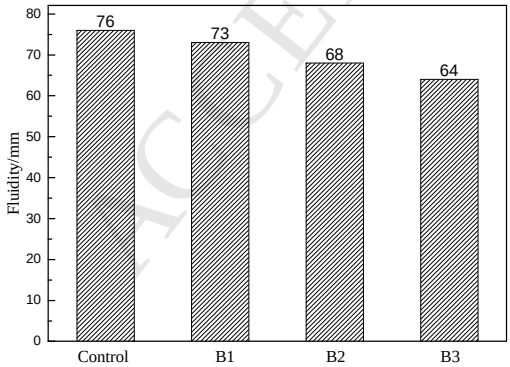

Fig. 8. Fluidity of cement pastes.

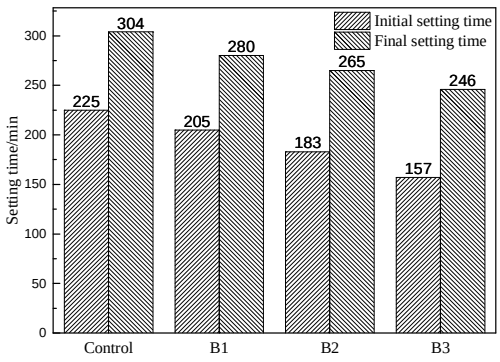

Fig. 9. Setting time of cement pastes.

3.3 Compressive strength of cement paste

Compressive strength of PC pastes containing nano-$CaCO_3$ suspensions are indicated in Fig. 10. It

can be found that the compressive strength was generally improved after various curing days. When being compared with those of the control sample, the 3d, 7d, 28d and 56d compressive strength of specimens with nano-$CaCO_3$ suspensions were increased by 2.8~5.8%, 2.0~9.9%, 3.4~7.2% and 3.5~7.6% respectively. At the same curing age, mixture B3 behaved the best improvement effect due to the highest nano-$CaCO_3$ content (Bentz et al., 2012).

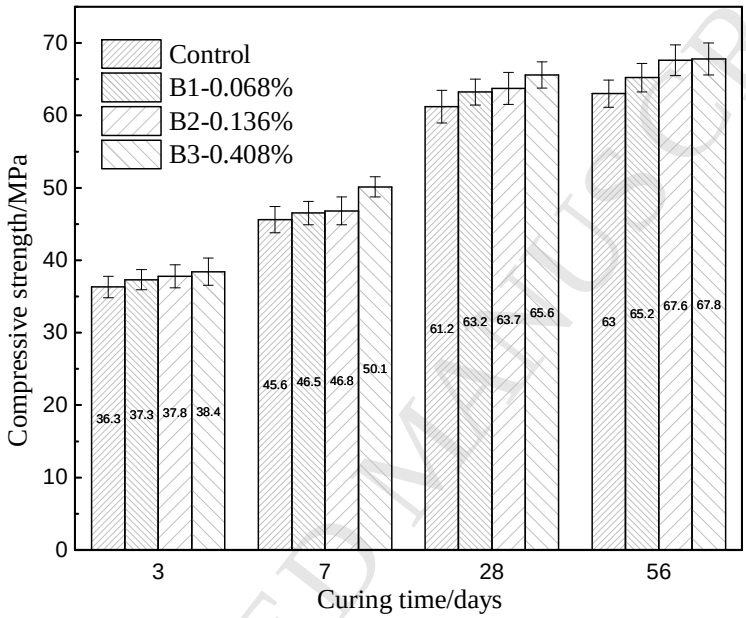

Fig. 10. Compressive strength of cement pastes.

It was reported that compressive strength of cement paste was increased by 20%~25% with 0.5%~2% addition of nanosilica by cement weight (Singh et al., 2013). Nevertheless, it was also observed that the 28-day compressive strength of cement paste was decreased by 8.57% with 3.8% addition of nanosilica (Berra et al., 2012). As for the carbonation curing of cement concretes, it was found that the 28-day compressive strength of carbonated concrete was decreased by 9.22% due to the water loss during carbonation curing (El-Hassan and Shao, 2015). Moreover, mixtures with fly ash behaved a lower 90-day strength as the pozzolanic reaction was probably hindered by the decreased $Ca(OH)_2$ content induced by carbonation curing (Zhang et al., 2016). Excessive carbonation sometimes caused adverse effects on early age strength of carbonated cement specimens (Junior et al., 2015). Even

238 though the compressive strength improvement induced by the addition of nano-$CaCO_3$ suspensions in
239 this study is not so significant as that of 0.5%~2% addition of nanosilica. This method of capturing
240 CO_2 addresses the limitations of carbonation curing and provides an innovative approach, being
241 beneficial to both environmental protection and performance improvement of Portland cement. The
242 increasing incorporation of nano-$CaCO_3$ can be achieved by the application $Ca(OH)_2$ solution with a
243 higher concentration and adjustable injection of CO_2, and then the better improvement on mechanical
244 strength of Portland cement paste is possibly obtained. These trials will be further investigated in
245 future.

246 3.4 Hydration heat of cement paste

247 The influence of nano-$CaCO_3$ suspension on hydration heat of cement paste is presented in Fig. 11.
248 There are three peaks for every hydration heat flow curve. The first peak is located at around 0~2 h,
249 being attributed to the ettringite (AFt) formation from tricalcium aluminate (C_3A) and the fast
250 dissolution of C_3S immediately after cement and water were in contact (Rupasinghe et al., 2017). The
251 second peak (at around 10~13 h) is induced by the accelerating consumption of C_3S and the
252 corresponding formation of C-S-H and $Ca(OH)_2$ (Saoût et al., 2013). The third peak with a shoulder
253 like shape located at around 13~17 h, being commonly attributed to the renewed hydration of C_3A
254 (Hesse et al., 2011; Saoût et al., 2013). During the accelerating period (prior to the second peak), the
255 more incorporation of nano-$CaCO_3$ led to the higher hydration heat rate. Therefore, the second peak
256 presented a higher value for samples containing B1 and B2 and it occurred earlier for sample
257 containing B3 than for the control sample. According to Fig. 11 (b), the total hydration heat was
258 increased by 1.4%, 1.6% and 4.9% respectively for mixtures containing B1, B2 and B3 when being
259 compared with the control sample. This accelerated hydration of cement paste accords with the

shortened setting time and improved strength as described in Part 3.2 and 3.3.

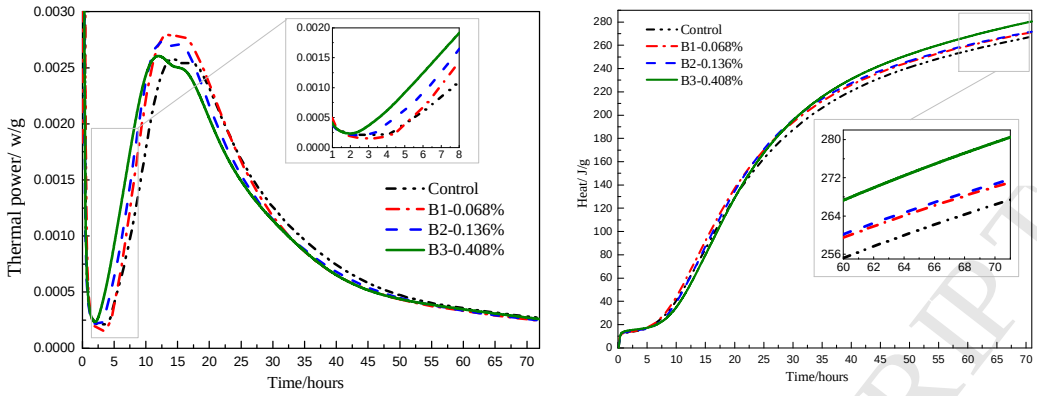

(a) Heat flow curve (b) Cumulative heat

Fig. 11. Hydration heat of cement pastes.

The accelerating effect of nano-$CaCO_3$ on cement hydration is commonly explained by the seeding effect (Rupasinghe et al., 2017). The existence of Nano-$CaCO_3$ particles near C_3S surfaces affects the induction period as indicated in Fig. 12. A protective layer of hydration products formed around C_3S particle leads to the low reaction rate during the induction period as shown in Fig. 12 (a). However, weakened spots are induced in this protective layer by nano-$CaCO_3$ particles as shown in Fig. 12 (b) (Sato and Diallo, 2010). The pore solution with a high Ca^{2+} concentration gets access to C_3S particle surface via these weakened and broken spots and subsequently rapid growth of C-S-H gel occurs (Glasser, 1979). In addition, the formation of calcium carboaluminate due to the chemical reaction between $CaCO_3$ and C_3A is another reason for the increased hydration rate and better early age strength (Moon et al., 2017).

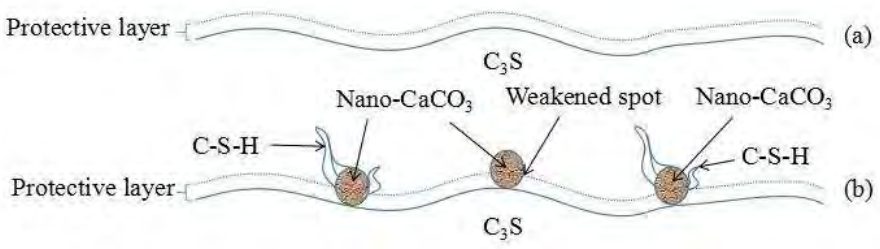

Fig. 12. Accelerating effect of nano-$CaCO_3$ on C_3S hydration.

3.5 XRD patterns of cement paste

To identify mineral composition of hydrated cement pastes containing different levels of nano-$CaCO_3$, XRD measurements were carried out on samples after 3d, 7d, 28d and 56d ages as shown in Fig. 13. Crystal substances for hardened PC samples are primarily composed of belite (C_2S), alite (C_3S), $Ca(OH)_2$ and AFt (Rupasinghe et al., 2017). C-S-H is the expected primary hydration product. But no characteristic peaks in XRD patterns can be attributable to C-S-H due to its amorphousness (Hu, 2017). No visible peaks are attributable to carboaluminate, possibly due to the small dose of $CaCO_3$ incorporated in these cement pastes. The occurrence of $CaCO_3$ is attributed to both the carbonation of the specimen surface (Ho et al., 2018) and the added nano-$CaCO_3$ suspension. The intensities of C_3S/C_2S peaks were decreased by the addition of nano-$CaCO_3$ suspension (especially at early ages), indicating that the existence of nano-$CaCO_3$ accelerated the hydration of C_3S and C_2S as verified by the above hydration heat results (Cao et al., 2014). With the increase of curing ages, the intensities of C_3S/C_2S peaks become weaker due to the ongoing hydration process of Portland cement throughout the entire curing ages (Land and Stephan, 2018). What's more, the content of the hydration product $Ca(OH)_2$ in B1~B3 specimens is more than that in the control sample, providing another evidence for the hydration accelerating effect.

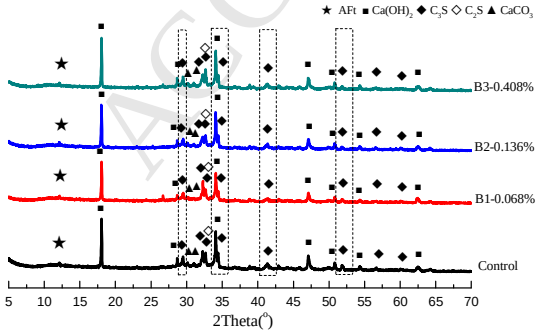

(a) 3 d

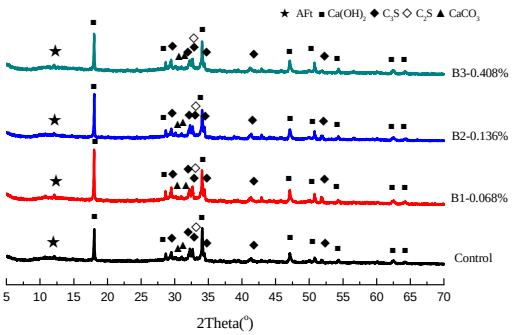

(b) 7 d

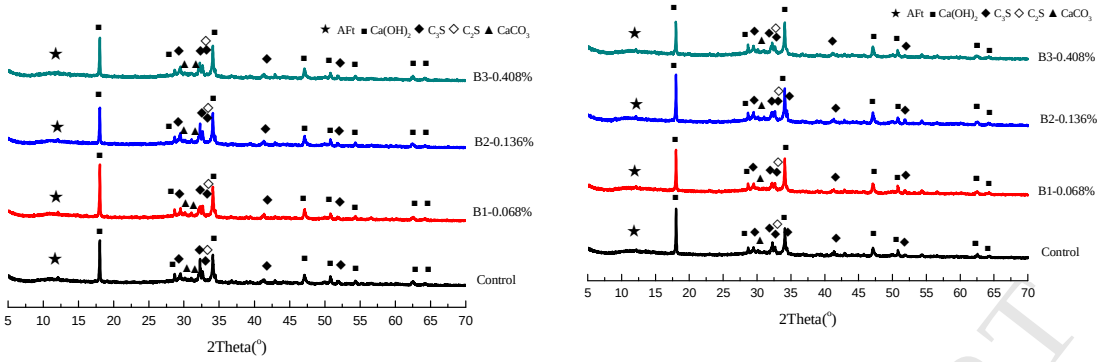

(c) 28d (d) 56d

290 Fig. 13. XRD patterns of cement pastes at various ages.

291 3.6 FTIR spectrum of cement paste

292 The FTIR spectrum was acquired for every hardened cement paste with different curing ages as

293 shown in Fig. 14. The vibrational band at 3420 cm^{-1} is originated from the O-H bond in H_2O. The

294 bands observed at 875 and 1430 cm^{-1} are assigned to C-O band in the form of CO_3^{2-}. Besides, the

295 vibrational band at 3640 cm^{-1} is originated from the O-H bond in the form of OH^- and the weak

296 absorption peak at 1640 cm^{-1} is also assigned to the bending band of O-H groups in water (Qin et al.,

297 2018). The peaks located at 450 cm^{-1}, 975 cm^{-1} indicate the presence of Si-O bending band attributed to

298 C-S-H gel (Li and Liu, 2018). Generally, different level of nano-$CaCO_3$ had little influence on FTIR

299 spectrum, indicating that no formation of new chemical groups was induced.

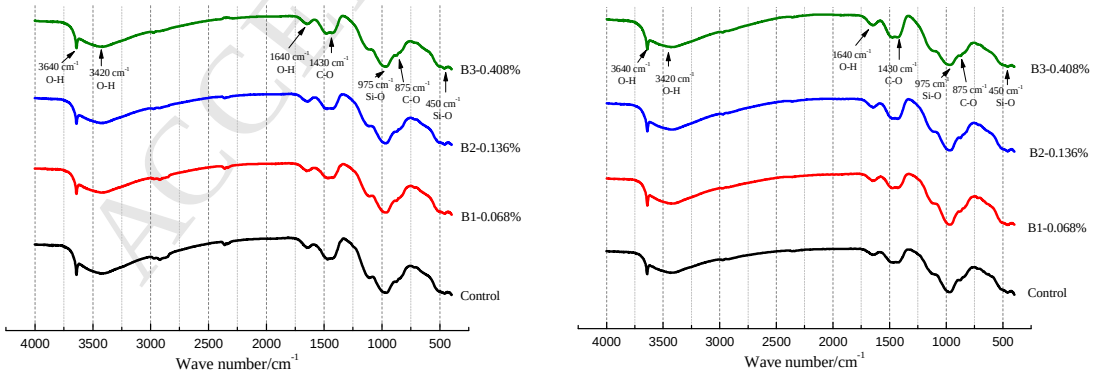

(a) 3d (b) 7d

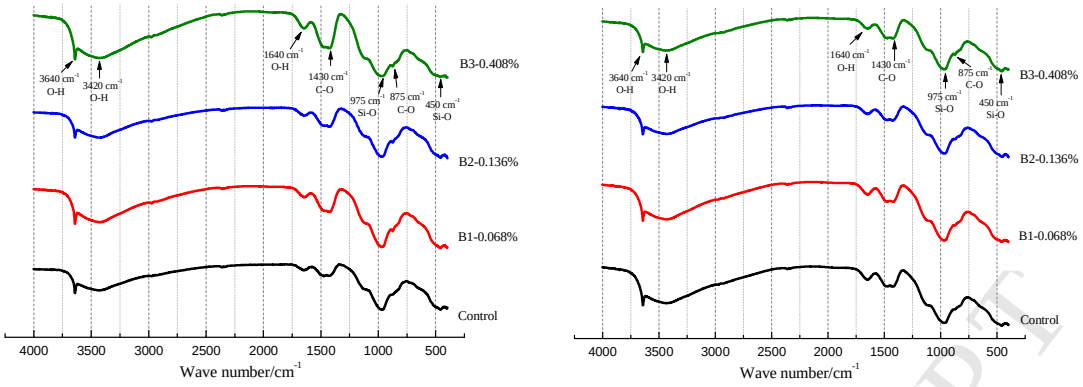

(c) 28d (d) 56d

Fig. 14. FTIR spectra of cement pastes at various ages.

3.7 TG-DTA analysis of cement paste

Fig. 15 illustrates TG-DTA curves for hardened pastes containing different nano-$CaCO_3$ suspensions after various ages of curing. It is evidently observed that every sample exhibited two obvious endothermal peaks at temperatures of 450 ℃ and 700 ℃, being attributed to the decomposition of $Ca(OH)_2$ and $CaCO_3$ respectively (Mo et al., 2016; Rostami et al., 2012). Based on the induced weight losses at the temperature range of 420~540 ℃ and 540~950 ℃, the amount of $Ca(OH)_2$ and $CaCO_3$ can be roughly calculated. The calculated content of $Ca(OH)_2$ in each cement paste sample at dry state is presented in Fig. 16. Being compared with the control sample, the $Ca(OH)_2$ content was increased by 11.90%~46.43% with the incorporation of nano-$CaCO_3$ suspensions. Among these three samples, B3 had the best improvement effect. It is well known that the amount of $Ca(OH)_2$ in a hydrated cement paste reflects the hydration degree of cement system (Sato and Diallo, 2010). Therefore, the increasing trend of $Ca(OH)_2$ amount is related to the accelerated hydration reaction of cement as proved by the hydration heat flow in Part. 3.3. With the increasing curing age, a higher content of $Ca(OH)_2$ formed in every sample due to the continued hydration reaction but the improvement effect of nano-$CaCO_3$ suspensions slightly decreased.

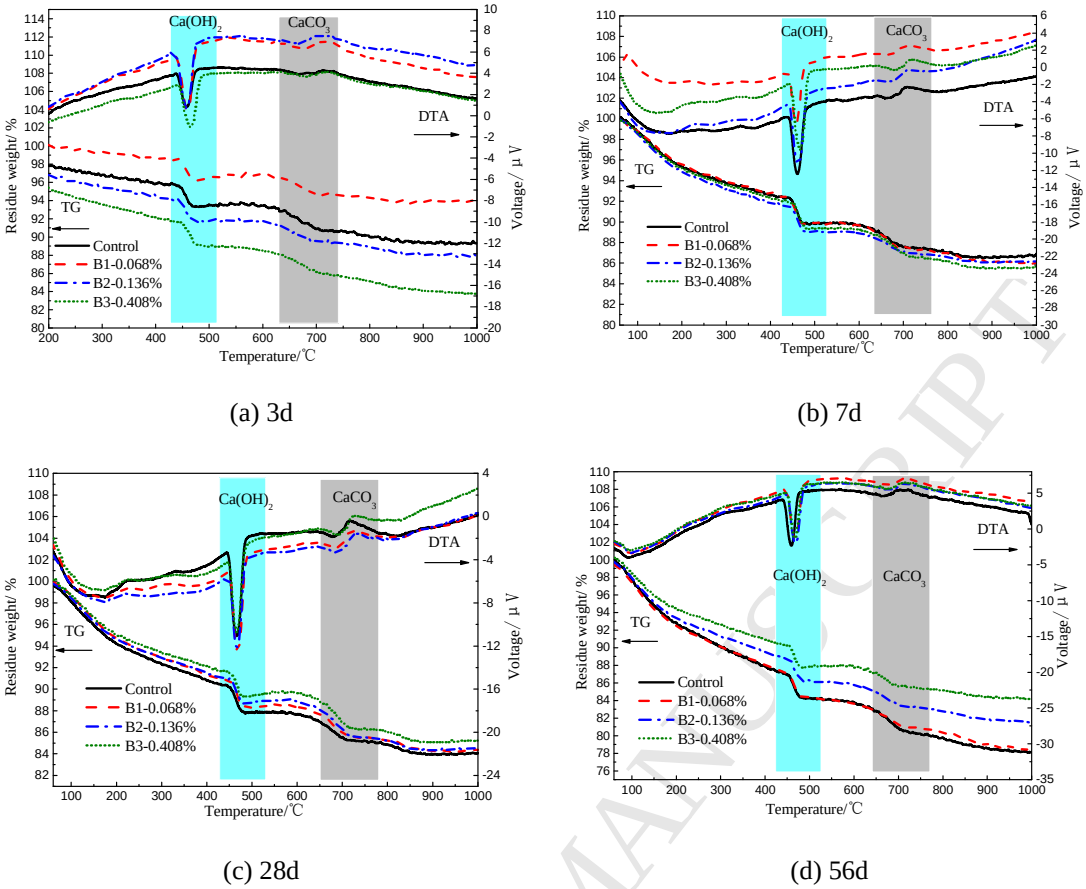

(a) 3d (b) 7d

(c) 28d (d) 56d

316 Fig. 15. TG-DTA curves of PC pastes at various ages.

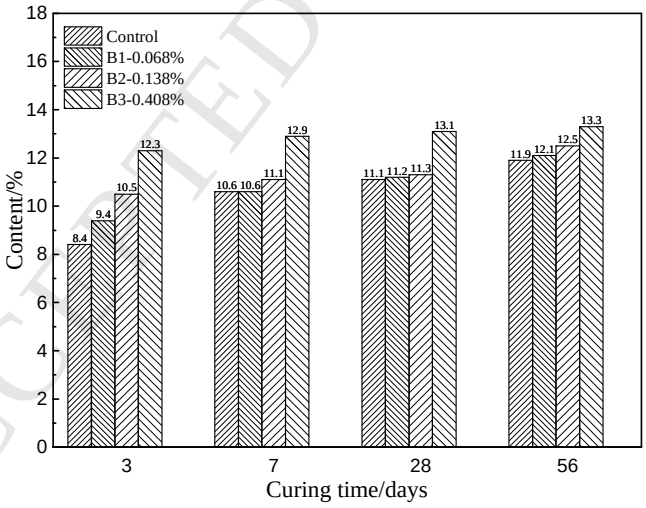

317

318 Fig. 16. $Ca(OH)_2$ content in cement pastes at various ages.

319 3.8 Pore structure of cement paste

320 The pore structures for selected samples were measured by the MIP method in this study. The

321 differential curves are presented in Fig. 17 and typical pore parameters are indicated in Table 4. It can

322 be found that B1~B3 specimens had a less content of coarse pores with diameter bigger than 100 nm

than the control sample. And the total porosity was also decreased by the incorporation of nano-$CaCO_3$. This is due to the higher hydration degree and contributes significantly to the improved mechanical strength. Specifically, the porosity of cement paste after 3d, 7d, 28d and 56d was decreased by 4.6~5.6%, 5.7~7.4%, 7.1~8.7% and 9.8~13.5% respectively due to the incorporation of nano-$CaCO_3$ suspensions. Besides, the porosity of all specimens decreased with the increase of curing age as expected and the compactness growth developed very slowly at later ages (Mo et al., 2016; Mo and Panesar, 2012).

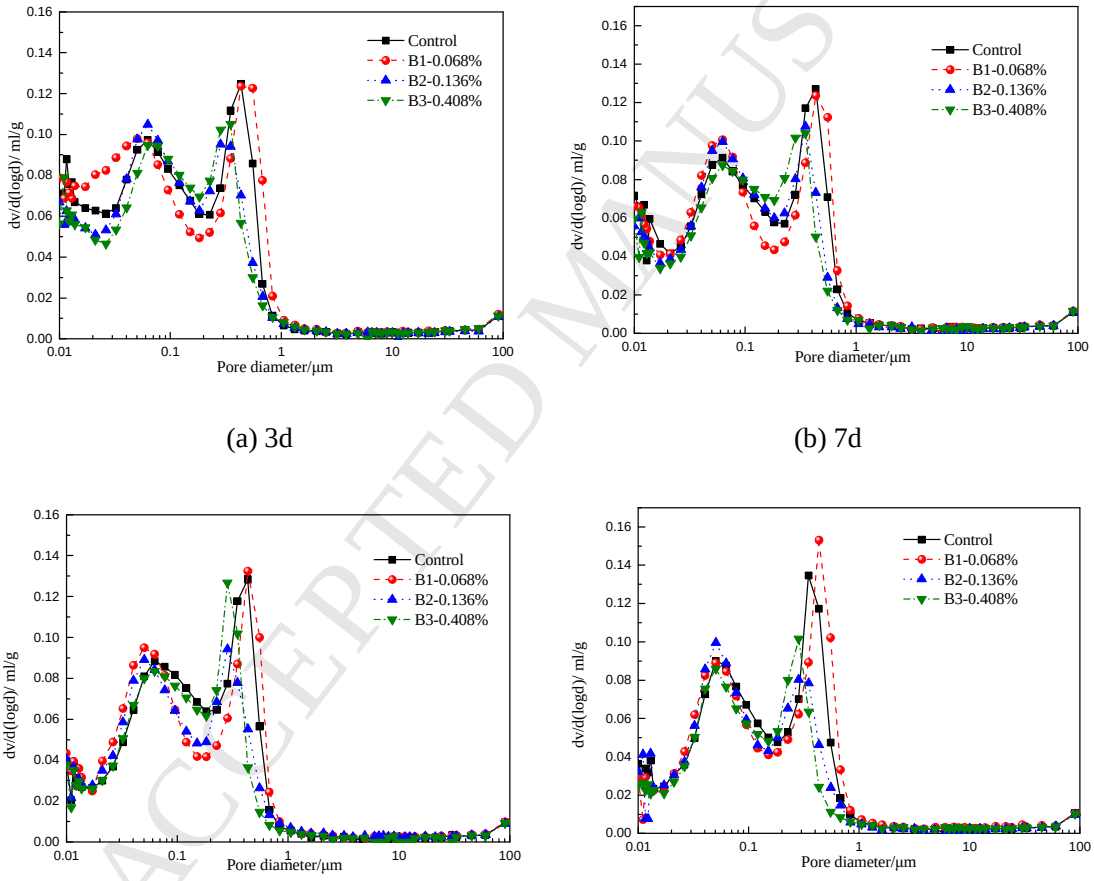

(a) 3d (b) 7d

(c) 28d (d) 56d

Fig. 17. Pore size distribution of PC pastes at various ages.

Table 4 Pore structure parameters of PC pastes.

Curing days	Group	Porosity（%）	Pore size distribution（%）			
			<20nm	20～50nm	50～100nm	>100nm
3d	Control	30.2	19.0	15.4	15.3	50.3

	B1	30.8	18.5	17.5	15.4	48.6
	B2	28.8	18.6	16.9	16.7	47.8
	B3	28.5	19.0	20.7	13.5	46.8
7d	Control	28.2	18.1	14.4	15.7	51.8
	B1	28.0	19.1	15.8	16.2	48.9
	B2	26.6	18.1	15.6	17.4	48.9
	B3	26.1	20.0	19.3	13.4	47.3
28d	Control	25.4	13.4	13.4	16.2	57.0
	B1	25.3	16.1	15.3	15.2	53.4
	B2	23.2	14.6	17.1	17.0	51.3
	B3	23.6	15.0	17.6	17.5	49.9
56d	Control	24.4	9.7	16.6	16.4	57.3
	B1	24.5	15.2	16.8	14.9	53.1
	B2	22.0	12.8	17.2	18.3	51.7
	B3	21.1	13.3	18.2	19.8	48.7

3.9 SEM observation of cement paste

SEM observations were carried out on selected samples as shown in Fig. 18. The mineral compositions in labelled regions were confirmed by EDS analysis. There are some unhydrated C_3S and a trace of $Ca(OH)_2$ crystals existing in the control specimen after 3 days curing. For B3 specimen, many hexagonal plate-like $Ca(OH)_2$ with size of about 8 μm can be observed, being attributed to the accelerated effect of nano-$CaCO_3$ on hydration of cement as described in Part 3.7. With the prolonging age, some needle-like ettringite (AFt) crystals were observed in both the control and B3 specimens. Furthermore, the microstructure of nano-$CaCO_3$ added specimen looks denser than that of the control sample, resulting in the higher compressive strength as described above.

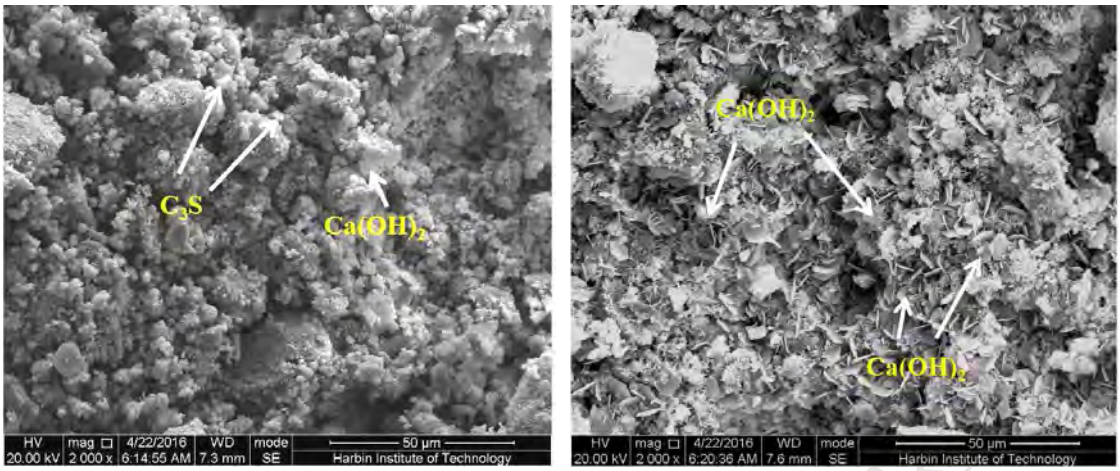

(a) Control 3d (×2000) (b) B3 3d (×2000)

(c) Control 28d (×5000) (d) B3 28d (×5000)

Fig. 18. SEM observation for selected hardened cement pastes.

3.10 Environmental benefit analysis

From the above experimental results, the absorption amount of CO_2 reached 0.0404%~0.2426% of Portland cement by weight with this upcycling method and the 28 days strength of cement paste was increased by 3.4~7.2%. This means that an estimated 1.86~11.2 million tons of CO_2 can be recycled by the annual production of cement all over the world (4.6 billion tons) without any negative effects, being a great contribution to reduce the greenhouse gas release. This contribution maybe greater when a higher dosage of the manufactured nano-$CaCO_3$ is incorporated in further studies. On the other hand, the increase of mechanical strength has a great potential to reduce the cement amount or reuse a higher

level of industrial wastes as mineral admixtures such as fly ash and ground granulated blast furnace slag (Monkman and Macdonald, 2017). It is reported that every ton of Portland cement has an emission of 1040 kg CO_2 (Portland Cement Association, 2016). Therefore, the cement producer can in situ upcycle the released CO_2 for manufacturing the nano-$CaCO_3$ suspension as a mineral agent for concrete, being accordance with the roles of circular economy and environmental protection.

4. Conclusions

Based on the above experimental results, the following conclusions can be obtained.

(1) A novel method was developed to upcycle CO_2 for manufacturing nano-$CaCO_3$ suspension by injecting CO_2 into $Ca(OH)_2$ solution. The produced $CaCO_3$ presented spherical and cubic particles with size of 20 to 50 nm.

(2) The manufactured nano-$CaCO_3$ suspension increased the 3d, 7d, 28d and 56d compressive strength by 2.8~5.8%, 2.0~9.9%, 3.4~7.2% and 3.5~7.6% respectively. The initial and final setting times were reduced by 8.89%~30.22% and 7.89%~19.08% respectively.

(3) The early age hydration of Portland cement was accelerated by the nano-$CaCO_3$ suspension, resulting in the increased hydration heat release and more formation of $Ca(OH)_2$ in hardened cement paste.

(4) With introduction of the nano-$CaCO_3$ suspension, the porosity was reduced and the pore structure was refined for the hardened cement pastes.

(5) Each ton of Portland cement absorbed around 0.4~2.4 kg of CO_2 while the usage efficiency of cement was improved by around 3.4~7.2%. Therefore, this upcycling method has a great environmental potential being attributed to both the capture and solidification of carbon dioxide and the carbon footprint reduction of cement industry.

(6) This technology has a potential for capturing variable industrial emissions with high concentration of CO_2 which needs more studies. On the other hand, the $Ca(OH)_2$ solution can be replaced by calcium-rich wastes such as slaked lime slurry and calcium carbide slag to achieve a better environmental effect.

Acknowledgments

The authors would like to acknowledge the financial support of the National Natural Science Foundation of China (No. 51778188) and the Practical Technology Research and Development Program of Heilongjiang Province-China [GA16C103].

References

Ashraf, W., 2016. Carbonation of cement-based materials: challenges and opportunities. Constr. Build. Mater 120, 558-570. https://doi.org/10.1016/j.conbuildmat.2016.05.080.

Ahmad, S., Assaggaf, R.A., Maslehuddin, M., Al-Amoudi, O.S.B., Adekunle, S.K., Ali, S.I., 2017. Effects of carbonation pressure and duration on strength evolution of concrete subjected to accelerated carbonation curing. Constr. Build. Mater. 136, 565-573. https://doi.org/10.1016/j.conbuildmat.2017.01.069.

Asikin-Mijan, N., Taufiq-Yap, Y.H., Lee, H.V., 2015. Synthesis of clamshell derived $Ca(OH)_2$ nano-particles via simple surfactant-hydration treatment. Chem. Eng. J. 26, 1043-1051. https://doi.org/10.1016/j.cej.2014.10.069.

Brouwers, H.J.H., 2008. Natural stone waste powders applied to scc mix design. Restor. Build. Monum. 14(2), 131-140. https://doi.org/10.1515/rbm-2008-6206.

Biernacki, J.J., Bullard, J.W., Sant, G., Brown, K., Glasser, F.P., Jones, S., Ley, T.R., 2017. Cements in the 21st century: challenges, perspectives, and opportunities. J. Am. Ceram. Soc. 100, 2746-2773.

https://doi.org/10.1111/jace.14948.

Berra, M., Carassiti, F., Mangialardi, T., Paolini, A.E., Sebastiani, M., 2012. Effects of nanosilica addition on workability and compressive strength of portland cement pastes. Constr. Build. Mater. 35, 666-675. https://doi.org/10.1016/j.conbuildmat.2012.04.132.

Brouwers, H.J.H., Radix, H.J., 2005. Self-compacting concrete: theoretical and experimental study. Cem. Concr. Res. 35(11), 2116-2136. https://doi.org/10. 1016/j.cemconres.2005.06.002.

Benhelal, E., Rashid, M.I., Holt, C., Rayson, M.S., Brent, G., Hook, J.M., 2018. The utilisation of feed and byproducts of mineral carbonation processes as a pozzolanic cement replacements. J. Cleaner. Prod. 186, 499-543. https://doi.org/10.1016/j.jclepro.2018.03.076.

Bentz, D.P., Sato, T., Varga, I.D.L., Weiss, W.J., 2012. Fine limestone additions to regulate setting in high volume fly ash mixtures. Cem. Concr. Compos. 34(1), 11-17. https://doi.org/10.1016/j.cemconcomp.2011.09.004.

Bourtsalas, A.C., Zhang, J., Castaldi, M.J., Themelis, N.J., 2018. Use of non-recycled plastics and paper as alternative fuel in cement production. J. Cleaner. Prod. 181, 8-16. https://doi.org/10.1016/j.jclepro.2018.01.214.

CEMBUREAU, 2016. Activity Report 2015. European Cement Association, Brussels.

Cai, Y., Hou, P., Cheng, X., Du, P., Ye, Z., 2017. The effects of nano-SiO_2, on the properties of fresh and hardened cement-based materials through its dispersion with silica fume. Constr. Build. Mater. 148, 770-780. https://doi.org/10.1016/j.conbuildmat.2017.05.091.

Carvalho, S.Z., Vernilli, F., Almeida, B., Oliveira, M.D., Silva, S.N., 2017. Reducing environmental impacts: the use of basic oxygen furnace slag in portland cement. J. Cleaner. Prod. 172, 385-390. https://doi.org/10.1016/j.jclepro.2017.10.130.

417 Cao, M., Zhang, C., Lv, H., Xu, L., 2014. Characterization of mechanical behavior and mechanism of
418 calcium carbonate whisker-reinforced cement mortar. Constr. Build. Mater. 66(1), 89-97.
419 https://doi.org/10.1016/j.conbuildmat.2014.05.059.
420 Double, D.D., Hellawell, A., 1978. The hydration of portland cement. Nature, 359(1699), 435-451.
421 http://dx.doi.org/10.1038/261486a0.
422 Du, Y., Meng, Q., Hou, R., Yan, J., Dai, H., Zhang, T., 2012. Fabrication of nano-sized $Ca(OH)_2$, with
423 excellent adsorption ability for N_2O_4. Particuology. 10(6), 737-743.
424 El-Sheikh, S.M., El-Sherbiny, S., Barhoum, A., Deng, Y., 2013. Effects of cationic surfactant during the
425 precipitation of calcium carbonate nano-particles on their size, morphology, and other
426 characteristics. Colloids Surf. A. 422(7), 44-49. https://doi.org/10.1016/j.colsurfa.2013.01.020.
427 El-Hassan, H., Shao, Y., 2015. Early carbonation curing of concrete masonry units with portland
428 limestone cement. Cem. Concr. Compos. 62, 168-177.
429 https://doi.org/10.1016/j.cemconcomp.2015.07.004.
430 Glasser, L.S.D., 1979. Osmotic pressure and the swelling of gels. Cem. Concr. Res. 9(4), 515-517.
431 https://doi.org/10.1016/0008-8846(79)90050-4.
432 Hesse, C., Goetz, N.F., Neubauer, J., 2011. A new approach in quantitativein-situ XRD of cement
433 pastes: correlation of heat flow curves with early hydration reactions. Cem Concr Res. 41,
434 123-128. https://doi.org/10.1016/j.cemconres.2010.09.014.
435 Ho, L.S., Nakarai, K., Ogawa, Y., Sasaki, T., Morioka, M., 2018. Effect of internal water content on
436 carbonation progress in cement-treated sand and effect of carbonation on compressive strength.
437 Cem. Concr. Compos. 85, 9-21. https://doi.org/10.1016/j.cemconcomp.2017.09.016.
438 Hemalatha, T., Ramaswamy, A., 2017. A review on fly ash characteristics- towards promoting high

volume utilization in developing sustainable concrete. J. Clean. Prod. 147, 546-559. https://doi.org/10.1016/j.jclepro.2017.01.114.

Hu, J., 2017. Comparison between the effects of superfine steel slag and superfine phosphorus slag on the long-term performances and durability of concrete. J. Therm. Anal. Calorim. 128, 1-13. https://doi.org/10.1007/s10973-017-6107-9.

International Energy Agency, 2008. In: Energy Technology Perspectives 2008: Scenarios and Strategies to 2050. OECD, Paris.

Junior, A.N., Filho, R.D.T., Fairbairn, E.D.M.R., Dweck, J., 2015. The effects of the early carbonation curing on the mechanical and porosity properties of high initial strength Portland cement pastes. Constr. Build. Mater. 77, 448-454. https://doi.org/10.1016/j.conbuildmat.2014.12.072.

Jang, J.G., Kim, G.M., Kim, H.J., Lee, H.K., 2016. Review on recent advances in CO_2 utilization and sequestration technologies in cement-based materials. Constr. Build. Mater 127, 762-773. https://doi.org/10.1016/j.conbuildmat.2016.10.017.

Kashef-Haghighi, S., Ghoshal, S., 2013. Physico-chemical processes limiting CO_2 uptake in concrete during accelerated carbonation curing. Ind. Eng. Chem. Res. 52, 5529-5537. http://dx.doi.org/10.1021/ie303275e.

Kawashima, S., Hou, P., Corr, D.J., Shah, S.P., 2013. Modification of cement-based materials with nanoparticles. Cem. Concr. Compos. 36(1), 8-15. https://doi.org/10.1016/j.cemconcomp.2012.06.012.

Kawashima, S., Hou, P., Corr, D.J., Shah, S.P., 2013. Modification of cement-based materials with nanoparticles. Cem. Concr. Compos. 36(1), 8-15. http://dx.doi.org/10.1016/j.cemconcomp.2012.06.012.

461 Li, F., Liu, J., 2018. An experimental investigation of hydration mechanism of cement with silicane.
462 Constr. Build. Mater. 166, 684-693. https://doi.org/10.1016/j.conbuildmat.2018.01.164.
463 Liu, J., Li, Q., Xu, S., 2015. Influence of nanoparticles on fluidity and mechanical properties of cement
464 mortar. Constr. Build. Mater. 101, 892-901. https://doi.org/10.1016/j.conbuildmat.2015.10.149.
465 Land, G., Stephan, D., 2018. The effect of synthesis conditions on the efficiency of C-S-H seeds to
466 accelerate cement hydration. Cem. Concr. Compos. 87, 73-78.
467 https://doi.org/10.1016/j.cemconcomp.2017.12.006.
468 Liu, X., Zhou, J., Zhang, Y.B., Liu, X.N., Chen, Y.L., 2015. Continuous process of biogas purification
469 and co-production of nano calcium carbonate in multistage membrane reactors. Chem. Eng. J. 271,
470 223-231. https://doi.org/10.1016/j.cej.2015.02.086.
471 Madani, H., Bagheri, A., Parhizkar, T., 2012. The pozzolanic reactivity of monodispersed nanosilica
472 hydrosols and their influence on the hydration characteristics of Portland cement. Cem Concr Res.
473 42(12), 1563-1570. https://doi.org/10.1016/j.cemconres.2012.09.004.
474 Monkman, S., Macdonald, M., 2017. On carbon dioxide utilization as a means to improve the
475 sustainability of ready-mixed concrete. J. Clean. Prod. 167, 365-375.
476 https://doi.org/10.1016/j.jclepro.2017.08.194.
477 Moon, G.D., Oh, S., Sang, H.J., Choi, Y.C., 2017. Effects of the fineness of limestone powder and
478 cement on the hydration and strength development of PLC concrete. Constr. Build. Mater. 135,
479 129-136. https://doi.org/10.1016/j.conbuildmat.2016.12.189.
480 Mo, L., Panesar, D.K., 2012. Effects of accelerated carbonation on the microstructure of portland
481 cement pastes containing reactive MgO. Cem. Concr. Res. 42(6), 769-777.
482 https://doi.org/10.1016/j.cemconres.2012.02.017.

Monkman, S., Shao, Y., 2010. Integration of carbon sequestration into curing process of precast concrete. Can. J. Civ. Eng. 37 (2), 302-310. https://doi.org/10.1139/L09-140.

Madlool, N.A., Saidur, R., Rahim, N.A., Kamalisarvestani, M., 2013. An overview of energy savings measures for cement industries. Renew. Sustain. Energy Rev. 19, 18-29. https://doi.org/10.1016/j.rser.2012.10.046.

Mo, L., Zhang, F., Deng, M., 2016. Mechanical performance and microstructure of the calcium carbonate binders produced by carbonating steel slag paste under CO_2 curing. Cem. Concr. Res. 88, 217-226. https://doi.org/10.1016/j.cemconres.2016.05.013.

Nazari, A., Riahi, S., 2011. The effects of SiO_2 nanoparticles on physical and mechanical properties of high strength compacting concrete. Composites. Part. B. 42, 570-578. https://doi.org/10.1016/j.compositesb.2010.09.025.

Portland Cement Association, 2016. Portland Cement Environmental Product Declaration [WWW Document]. URL. www.cement.org/epd (Accessed 13 April 17).

Qin, L., Gao, X., Chen, T., 2018a. Recycling of raw rice husk to manufacture magnesium oxysulfate cement based lightweight building materials. J. Clean. Prod. 191, 220-232. https://doi.org/10.1016/j.jclepro.2018.04.238.

Qin, L., Gao, X., Li, W., Ye, H., 2018b. Modification of magnesium oxysulfate cement by incorporating weak acids. J. Mater. Civ. Eng. (accept). https://doi.org/10.1061/(ASCE)MT.1943-5533.0002418.

Quercia, G., Hüsken, G., Brouwers, H.J.H., 2012. Water demand of amorphous nano silica and its impact on the workability of cement paste. Cem. Concr. Res. 42(2), 344-357. https://doi.org/10.1016/j.cemconres.2011.10.008.

505 Reddy, M.M., Nancollas, G.H., 1976. The crystallization of calcium carbonate: iv. the effect of
506 magnesium, strontium and sulfate ions. J. Cryst. Growth. 35(1), 33-38.
507 https://doi.org/10.1016/0022-0248(76)90240-2.
508 Rupasinghe, M., Nicolas, R.S., Mendis, P., Sofi, M., Ngo, T., 2017. Investigation of strength and
509 hydration characteristics in nano-silica incorporated cement paste. Cem. Concr. Compos. 80,
510 17-30. https://doi.org/10.1016/j.cemconcomp.2017.02.011.
511 Rostami, V., Shao, Y., Boyd, A.J., 2011. Carbonation curing versus steam curing for precast concrete
512 production. J. Mater. Civ. Eng. 24 (9), 1221-1229.
513 https://doi.org/10.1061/(ASCE)MT.1943-5533.0000462.
514 Rostami, V., Shao, Y., Boyd, A.J., He, Z., 2012. Microstructure of cement paste subject to early
515 carbonation curing. Cem. Concr. Res. 42(1), 186-193.
516 https://doi.org/10.1016/j.cemconres.2011.09.010.
517 Scrivener, K., 2014. Options for the future of cement. Indian Concr. J. 88, 11-21.
518 Sato, T., Beaudoin, J.J., 2011. Effect of nano-$CaCO_3$ on hydration of cement containing supplementary
519 cementitious materials. Adv. Cem. Res. 23(1), 33-43. https://doi.org/10.1680/adcr.9.00016.
520 Sato, T., Diallo, F., 2010. Seeding effect of nano-$CaCO_3$ on the hydration of tricalcium silicate. Transp.
521 Res. Rec. 2141(2141), 61-67. https://doi.org/61-67.10.3141/2141-11.
522 Shi, C., Jiménez, A.F., Palomo, A., 2011. New cements for the 21st century: the pursuit of an
523 alternative to portland cement. Cem. Concr. Res. 41(7), 750-763.
524 https://doi.org/10.1016/j.cemconres.2011.03.016.
525 Scrivener, K.L., John, V.M., Gartner, E.M., 2016. Eco-efficient Cements: Potential Economically
526 Viable Solutions for a Low-CO_2 Cement-based Materials Industry. United Nations Environment

Program, Paris.

Singh, L.P., Karade, S.R., Bhattacharyya, S.K., Yousuf, M.M., Ahalawat, S., 2013. Beneficial role of nanosilica in cement based materials-a review. Constr. Build. Mater. 47(5), 1069-1077. https://doi.org/10.1016/j.conbuildmat.2013.05.052.

Senff, L., Labrincha, J.A., Ferreira, V.M., Hotza, D., Repette, W.L., 2009. Effect of nano-silica on rheology and fresh properties of cement pastes and mortars. Constr. Build. Mater. 23(7), 2487-2491. http://dx.doi.org/10.1016/j.conbuildmat.2009.02.005.

Saoût, G.L., Lothenbach, B., Hori, A., Higuchi, T., Winnefeld, F., 2013. Hydration of portland cement with additions of calcium sulfoaluminates. Cem. Concr. Res. 43(1), 81-94. https://doi.org/10.1016/J.CEMCONRES.2012.10.011.

Schneider, M., Romer, M., Tschudin, M., Bolio, H., 2011. Sustainable cement production—present and future. Cem. Concr. Res. 41(7), 642-650. https://doi.org/10.1016/j.cemconres.2011.03.019.

Shao, Y., Rostami, V., He, Z., Boyd, A.J., 2014. Accelerated carbonation of portland limestone cement. J. Mater. Civ. Eng. 26(1), 117-124. https://doi.org/10.1061/(ASCE)MT.1943-5533.0000773.

Sanchez, F., Sobolev, K., 2010. Nanotechnology in concrete-a review. Constr. Build. Mater. 24, 2060-2071. https://doi.org/10.1016/j.conbuildmat.2010.03.014.

Vance, K., Falzone, G., Pignatelli, I., Bauchy, M., Balonis, M., Sant, G., 2015. Direct carbonation of $Ca(OH)_2$ using liquid and supercritical CO_2: implications for carbon-neutral cementation. Ind. Eng. Chem. Res. 54(36), 8908-8918. https://doi.org/10.1021/acs.iecr.5b02356.

Wadsö, L., Applications of an eight-channel isothermal conduction calorimeter for cement hydration studies. Cem Int. 2005;3:94-101.

Xi, L., Zhou, J., Zhang, Y., Liu, X., Chen, Y., Yong, X., 2015. Continuous process of biogas purification

549 and co-production of nano calcium carbonate in multistage membrane reactors. Chem. Eng. J. 271,

550 223-231. https://doi.org/10.1016/j.cej.2015.02.086.

551 Zhang, D., Cai, X., Shao, Y., 2016. Carbonation curing of precast fly ash concrete.J. Mater. Civ. Eng.

552 28(11), 04016127. https://doi.org/10.1061/(ASCE)MT.1943-5533.0001649.

553 Zhang, D., Ghouleh, Z., Shao, Y., 2017. Review on carbonation curing of cement-based materials. J.

554 CO_2. Util. 21, 119-131. https://doi.org/10.1016/j.jcou.2017.07.003.

555

Highlights

- Nano-$CaCO_3$ suspension was manufactured by upcycling CO_2.
- Compressive strength of Portland cement was increased by Nano-$CaCO_3$ suspension.
- Early age hydration was accelerated and pore structure was refined.
- Around 0.4~2.4 kg of CO_2 can be recycled by every ton of Portland cement.